

FRACTOGRAPHIC ANALYSIS OF FATIGUE FAILURE IN THE SUPERLONG LIFE REGIME OF $N > 10^7$ CYCLES

Yukitaka Murakami¹ and Toru Ueda² and Tetsushi Nomoto³

¹ Department of Mechanical Engineering, Kyushu University, 6-10-1
Hakozaki, Fukuoka, 812-8581, Japan

² Mitsubishi Heavy Industries, Ltd., 3-2-1 Gion Hiroshima, 730-0138, Japan

³ Mitsubishi Heavy Industries, Ltd., 1-1, Akunoura-machi, Nagasaki, 850-8610, Japan

ABSTRACT

The fracture surface of specimens of a heat treated hard steel, Cr-Mo steel SCM435, having failed in the order of $N = 10^5$ - 5×10^8 cycles were investigated by optical microscope, SEM and AFM. Specimens having longer fatigue lives had a particular morphology beside the inclusion at fracture origin. The particular morphology looked optically dark when observed by optical microscope and it was then named the optically dark area, ODA. It is shown directly or indirectly that ODA is made by the fatigue caused by cyclic stress with the synergetic effect of the hydrogen trapped by inclusion. The mechanism of the formation of ODA is suggested to be a key issue to solve the mechanism of superlong fatigue failure.

INTRODUCTION

The recent studies by Naito, Ueda and Kikuchi [1] and Asami and Sugiyama [2] have given to the existing knowledge a warning that fatigue failure occurs at the life regime longer than $N = 10^7$, i.e. $N = 10^8$ - 10^9 , at the stress lower than conventional fatigue limit. Recently similar studies followed those of Naito et al and the mechanism of the step wise S - N curve from low-cycle to extremely high cycle fatigue has been discussed by many researchers. Gigacycles ($N = 10^9$) corresponds to the cycles which a Japanese Shinkansen Train experiences during 10 years use. It is also very common that turbine blades experience more than $N = 10^7$ stress cycles by vibration.

If we imagine the many possible factors which may influence fatigue strength during such a long period of use, it is not so easy to identify the crucial mechanism. Miller and O'Donnell [3] and Murakami [4] discussed several possible factors which may cause fatigue failure in the regime of $N > 10^7$ cycles. Among several possible factors for eliminating the classical fatigue limit, Murakami et al pointed out the importance of the influence of the hydrogen trapped by nonmetallic inclusions [4]. The influence of hydrogen on static fracture such as hydrogen embrittlement and corrosion cracking has been well known. However, the influence of the hydrogen trapped by nonmetallic inclusions on fatigue failure in air has not been reported. This paper focuses on this particular problem by preparing specimens which contain different levels of hydrogen. It will be revealed that the fatigue fracture surfaces of the specimens containing different levels of hydrogen show very different fatigue fracture surface morphology and the influence of hydrogen is crucial for eliminating the fatigue limit in the cycle regime longer than the conventional fatigue test, i.e. $N > 10^7$.

THE METHOD OF DATA ANALYSIS

Fatigue fracture origins in extremely high cycle fatigue are mostly at nonmetallic inclusion. Therefore, this problem should be discussed from the viewpoint of small fatigue cracks. It has been well known that the threshold stress intensity factor ranges ΔK_{th} for small cracks are a function of crack size and lower than those for long cracks [5].

ΔK_{th} for small cracks and defects can be evaluated by the \sqrt{area} parameter model [6]:

$$K_{th} = 3.3 \times 10^{-3} (HV+120) (\sqrt{area})^{1/6} \quad (1)$$

$$\sigma_w = 1.43 (HV+120) / (\sqrt{area})^{1/6} \quad (2)$$

where, the units in the equations are ΔK_{th} : $\text{MPa}\cdot\text{m}^{1/2}$, the fatigue limit, σ_w : MPa, HV : kgf/mm^2 , and the square root of the projection area of a defect \sqrt{area} : μm .

The more general expressions [7] for Eqn. (1) or (2) for the stress ratio $R \neq -1$ are:

$$\text{Surface defects : } \sigma_w = 1.43 (HV+120) / (\sqrt{area})^{1/6} \cdot [(1-R)/2]^\alpha \quad (3)$$

$$\text{Internal defects : } \sigma_w = 1.56 (HV+120) / (\sqrt{area})^{1/6} \cdot [(1-R)/2]^\alpha \quad (4)$$

$$\text{where, } R \text{ (stress ratio)} = \sigma_{\min} / \sigma_{\max}, \quad (5)$$

$$\text{and } \alpha = 0.226 + HV \times 10^{-4} \quad (6)$$

If we compare the threshold values ΔK_{th} estimated by the \sqrt{area} parameter model for the results of $N_f > 10^7$ cycles with the experimental ΔK under which specimens failed, we may be able to find the causes which may influence fatigue strength in the regime of $N_f > 10^7$ cycles.

MATERIAL, SPECIMEN AND EXPERIMENTAL METHOD

The material used was a Cr-Mo Steel SCM435. The chemical composition (wt%) is 0.36C, 0.19Si, 0.77Mn, 0.014P, 0.006S, 0.08Ni, 1.0Cr, 0.15Mo, 0.13Cu and 8ppm O_2 . The loading was tension-compression with R ratio = -1. The following three different series of heat-treated specimens were prepared to investigate the influence of hydrogen:

(1) Specimen QT: The first series of specimens were quenched at 850°C and tempered at 170°C after carburizing and nitriding. These specimens are termed Specimen QT (Quenched & Tempered). The hardness of the core region of Specimen QT was approximately $HV = 560$.

(2) Specimen VA: The second and third series of specimens were prepared to investigate the influence of hydrogen trapped in the specimen. The second series of specimens were those which were annealed at 300°C in a vacuum. The specimens which were annealed for 1 hour at 300°C in a vacuum were termed Specimen VA1 and those which were annealed for 2 hours at 300°C in a vacuum were termed Specimen VA2. The hardness of the core region of Specimen VA was approximately $HV = 500$.

(3) Specimen VQ: The third series of specimens were those which were quenched in a vacuum under the same condition with Specimen QT except for the quenching environment. These specimens were termed Specimen VQ. The hardness distribution of Specimen VQ was almost the same as Specimen QT.

Before the fatigue tests, the content of hydrogen in Specimen QT and Specimen VQ was measured. The hydrogen content was 0.7-0.9ppm in Specimen QT and 0.01ppm in Specimen VQ.

Figure 1 shows the dimensions and shape of the tension compression fatigue specimens.

An oil-hydraulic-type closed-loop tension-compression fatigue testing machine operating at a frequency of 30 - 100Hz was used.

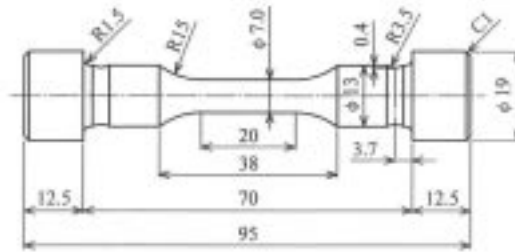


Figure 1: Shape and dimensions of the specimen; dimensions in mm.

RESIDUAL STRESS AND HARDNESS DISTRIBUTION

Compressive residual stress of approximately 500 MPa was present at the specimen surface. Figure 2 shows an example of hardness distribution at the cross section of a specimen QT. Figure 3 shows the distribution of the fatigue fracture origins on sections of specimens which are mostly distributed in the core region of the specimens due to lower hardness.

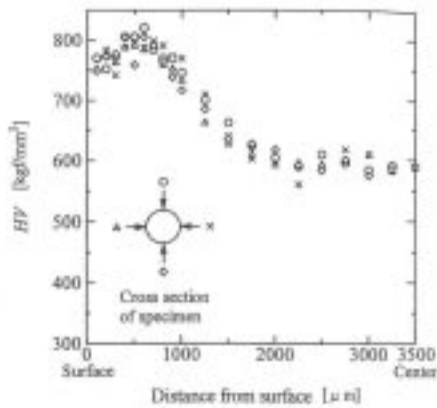


Figure 2: Hardness distribution across the section.

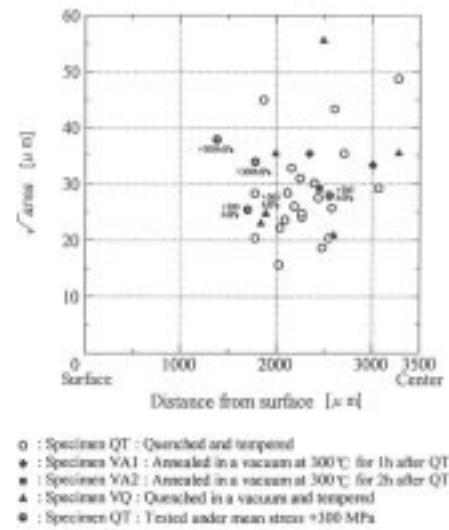
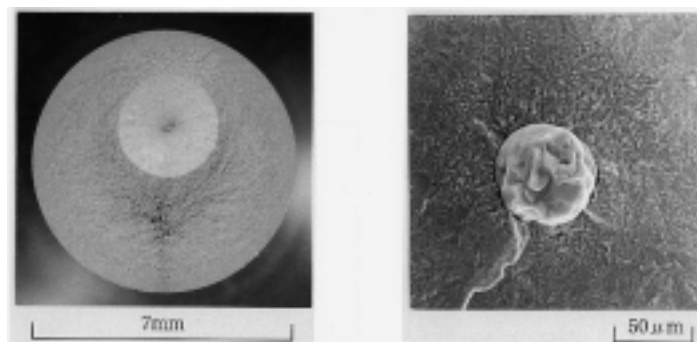


Figure 3: Size and radial distribution of the inclusions at the fracture origin.
The marks with +300 MPa means the specimen was tested under mean stress of +300 MPa.

FRACTURE ORIGINS

All fractures occurred from internal inclusions. The locations of these inclusions are at depths from the surface greater than 1700 μm . This is because the core of specimens is softer than the surface and the residual stress at the surface is compressive.

Figure 4 shows an example of a fish-eye fracture and the inclusion at the center of the fish-eye of a specimen QT. The inclusion was identified from an X-ray analysis of the chemical composition to be a $\text{Al}_2\text{O}_3 \cdot (\text{CaO})_x$ type globular duplex inclusion.



(a) Fish-eye topography (b) Inclusion at the center of fish-eye

Figure 4: Fish-eye topography and the inclusion at the center of fish-eye for a Specimen QT.

$$\sigma = 601 \text{ MPa}, N_f = 4.39 \times 10^7, \sqrt{\text{area}} = 25.7 \mu\text{m}$$

S-N CURVES

Figure 5 shows the $S-N$ data. The fracture origins of all specimens plotted in Fig. 5 are at internal inclusions and not at the surface.

In order to evaluate the influence of inclusions, the fatigue limit σ_w of each specimen was estimated by the \sqrt{area} parameter model, i.e. Eqn.(4), assuming a nonmetallic inclusion being equivalent to a small crack. Although the residual stress at the inclusion of the fracture origin is unknown, we give the stress ratio R a value of -1.0 for a tentative calculation, because the residual stress in the core region of specimen is thought to be very small.

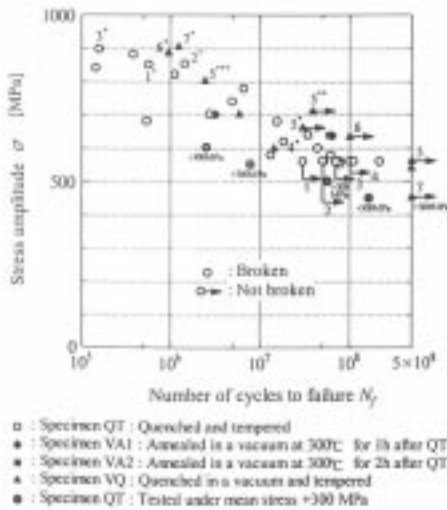


Figure 5: The $S-N$ data for Cr-Mo steel, SCM435. Fracture origins are all at nonmetallic inclusions. (The marks *, ** and *** indicate the specimen which ran out and was tested repeatedly at higher stress levels.)

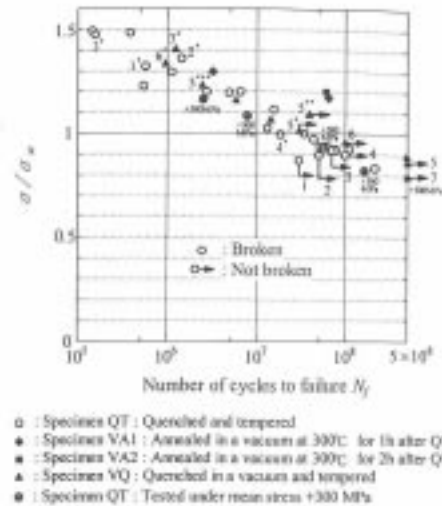


Figure 6: A type 1 modified $S-N$ data. σ = Stress amplitude. σ_w = Fatigue limit calculated by the \sqrt{area} parameter model.

The minimum value in the hardness distribution of $HV = 561$ (see Fig. 2) was used for our calculations.

Figure 6 shows a modified $S-N$ data, i.e. the relationship between the ratio of the applied stress to the estimated fatigue limit, σ/σ_w , and the cycles to failure N_f . Many specimens failed even at $\sigma/\sigma_w < 1.0$ and $N \geq 10^7$. These results show that the evaluations by the \sqrt{area} parameter model are approximately 10% unconservative predicting the fatigue limit for fatigue life time of $N_f = 10^8$ (approx.).

DETAILS OF FRACTURE SURFACE MORPHOLOGY AND INFLUENCE OF HYDROGEN

Figure 7 shows the optical micrographs of the fracture surface near the fracture origin for Specimen QT. If we carefully observe the center of the fish-eye mark with an optical microscope, we can find in most cases a dark area in the vicinity of the inclusion at the fracture origin [4] (see the illustration of Fig. 7(g)). This dark area was named ODA (Optically Dark Area) [8]. The size of ODA increases with the increase in fatigue life. It is interesting that ODA cannot be found on the fracture surface of specimens failed at a small number of cycles (see Fig. 7 (a)). According to the Scanning Electron Microscopy (SEM) observations, the ODA has a fracture surface quite different from that of the white area which shows a fatigue fracture surface typical of the structure of a martensite lath. Figure 8 shows the very rough morphology in a SEM observation [4] of the ODA. The observations of ODA by AFM also reveal a morphology that is very different from a typical fatigue fracture surface [4].

Figure 9 shows the relationship between the size of ODA and the cycles to failure. It is surprising that specimens having a longer life have a larger ODA relative to the original inclusion size as incorporated in the \sqrt{area} parameter [4]. This implies that fatigue failure after superlong high cycle fatigue beyond $N = 10^7$ cycles may be influenced by environmental conditions such as induced by H_2 . Fig. 9 includes also the data on a heat treated

medium carbon steel (0.46%C steel) which shows similar trends of increase in ODA with number of cycles to failure N_f .

Recently, Takai et al [9,10] directly verified the presence of the hydrogen trapped at the interface of inclusions by the Secondary Ion Mass Spectrometry (SIMS) (see Fig. 10). Takai et al showed that nonmetallic inclusions trapped hydrogen more strongly than other sites such as dislocations, grain boundaries and textures, and the hydrogen trapped by nonmetallic inclusions could be desorbed only by heating the sample at higher than $\sim 573\text{K}$.

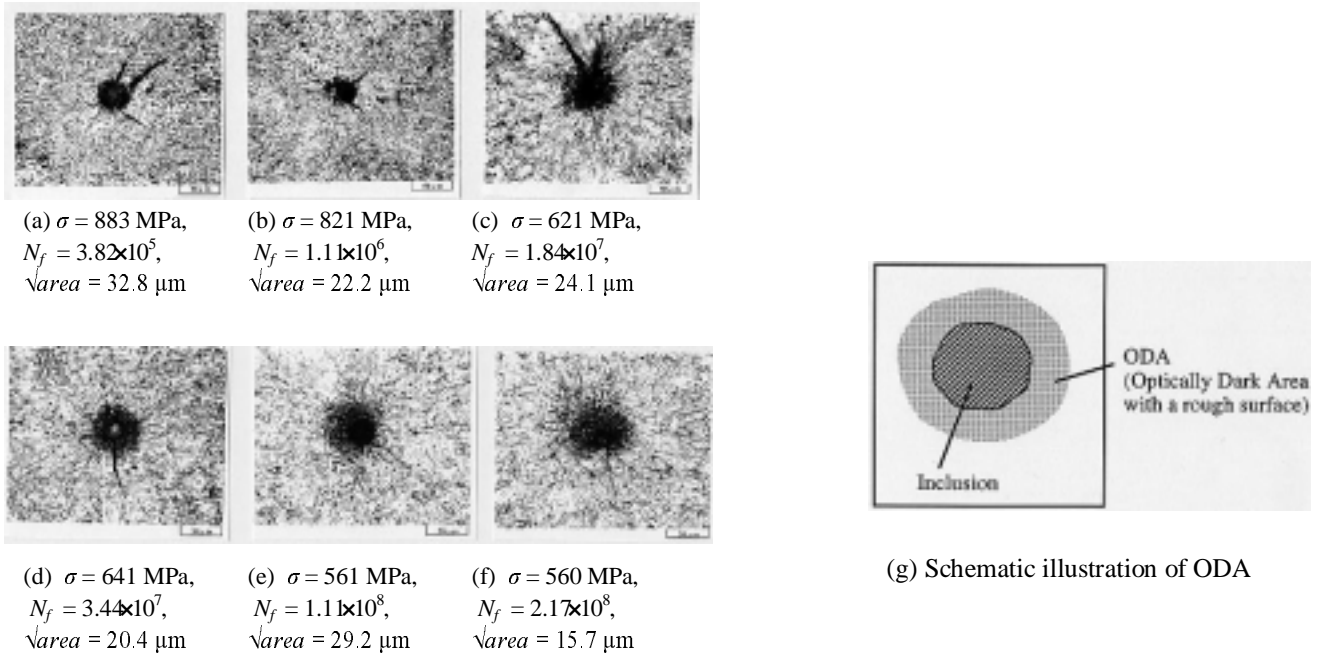


Figure 7: Optical micrographs of fracture surface near fracture origin from the life regime 10^5 cycles to 2×10^8 cycles. The size of dark area (Optically Dark Area, ODA) in the vicinity of inclusion at fracture origin increases with increase in fatigue life.

In the present material (Cr-Mo steel, SCM435), the total hydrogen content was measured to be 0.3-0.4ppm before heat treatment and 0.7-0.9ppm after the conventional quenching and tempering heat treatment of SCM435 (Specimen QT).

If we evaluate the effective size of an inclusion by adding the size of the dark area (ODA) to the original size of the inclusion, we can draw another modified $S-N$ diagram [4] as indicated in Fig. 11. Figure. 11 implies a hypothesis that after very slow fatigue crack growth inside ODA beside the inclusion, the size of the crack exceeds the critical size for the mechanical threshold value estimated by the $\sqrt{\text{area}}$ parameter model and then the fatigue crack grows without the assistance of hydrogen by producing a fatigue fracture surface typical to a martensite lath structure.

In order to verify this hypothesis, fatigue tests were carried out by using Specimens VA1, VA2 and VQ which contain less hydrogen ($\sim 0.01\text{ppm}$) than Specimen QT (0.7-0.9ppm). Specimens VA1 and VA2 were prepared by annealing Specimen QT at $300 \text{ }^\circ\text{C}$ for 1h and 2h in a vacuum respectively. Heating the specimen at $300 \text{ }^\circ\text{C}$ is necessary for desorbing the hydrogen trapped by inclusions. Specimens VQ were prepared by vacuum quenching.

The marks \blacklozenge and \blacksquare in Fig. 9 show the ODAs in Specimens VA1 and VA2 respectively. The mark \blacktriangle shows the ODAs in Specimen VQ. The ODAs in Specimens VA1 and VA2 are smaller than those for Specimen QT. The ODAs in Specimen VQ are much smaller than other specimens. Thus, we may conclude that the hydrogen trapped by inclusions crucially influences the formation of ODA, the particular fracture morphology around the inclusions at fracture origin. Although the coupling mechanism of hydrogen and cyclic stress is still not clear, the possible mechanism may be related to enhancing the mobility of screw and edge dislocations and reducing internal friction by hydrogen [11-18]. In this context, we may regard the influence of hydrogen on superlong fatigue as an internal environmental factor which a material contains in itself.

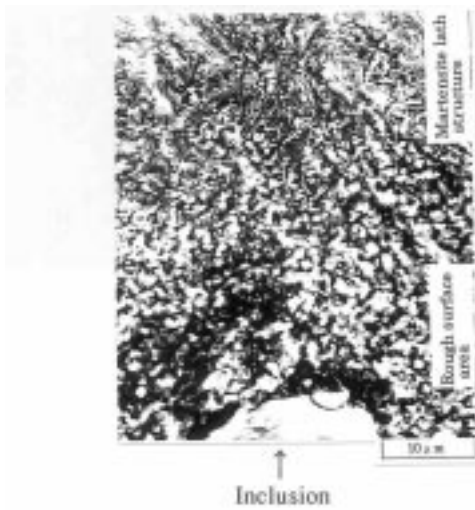


Figure 8: The dark area in the vicinity of inclusions at the fracture origin (Fig. 7(d)).

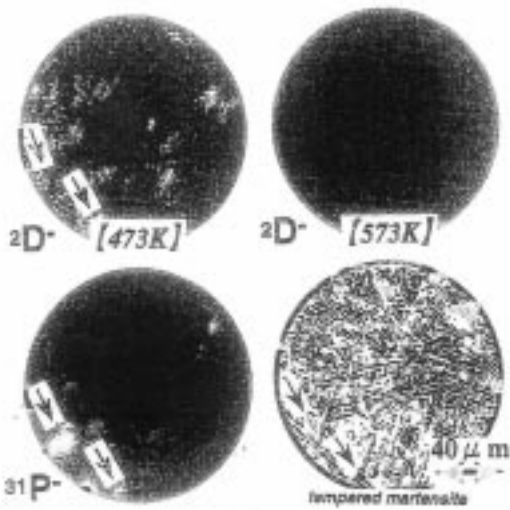
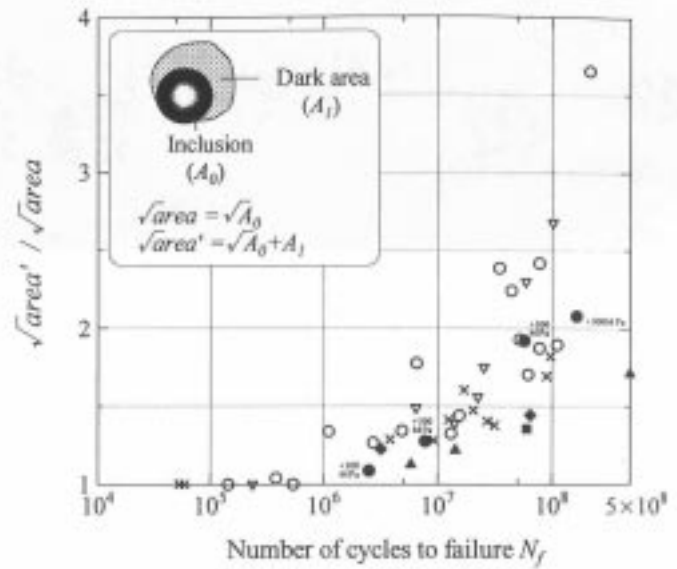


Figure 10: Evidences of the hydrogen trapped by nonmetallic inclusions. Secondary ion images of $^{2}\text{D}^-$ and $^{31}\text{P}^-$ after heating at 473K and 573K by TDS (Thermal Desorption Spectrometry), and optical microstructure of the PC bar (K. Takai et al [9]).



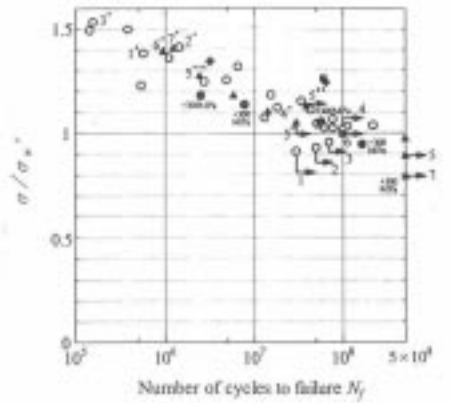
- : Specimen QT : Quenched and tempered
- ◆ : Specimen VA1 : Annealed in a vacuum at 300°C for 1h after QT
- : Specimen VA2 : Annealed in a vacuum at 300°C for 2h after QT
- ▲ : Specimen VQ : Quenched in a vacuum and tempered
- ▽ : HSL180 (Rotating-bending)
- × : S45C

$\sqrt{\text{area}}$: Inclusion size
 $\sqrt{\text{area}'}$: Inclusion size + the size of dark area

Figure 9: The relationship between the size of the Optically Dark Area and the cycles to failure. The open mark shows the ODAs in Specimen QT. The marks ◆ and ■ show the ODAs in Specimen VA1 and VA2 respectively. The mark ▲ shows the ODAs in Specimen VQ. The ODAs in Specimens VA1 and VA2 are smaller than those for Specimen QT. The ODAs in Specimen VQ are much smaller than other specimens.

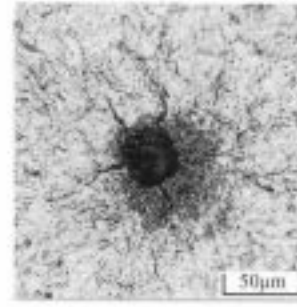
Other cases of fish-eye marks that were formed at other origins which are different from inclusions may support this hypothesis. Murakami et al [19] conducted rotary bending fatigue tests on a bearing steel produced by a special melting method. No ODA was observed beside the fracture origin in this particular case except for very rare cases in which nonmetallic inclusions became the fracture origin. The bearing steel was processed through a double electron beam remelting method and contained extremely small nonmetallic inclusions. In the bearing steel the size of the bainitic structure produced by local imperfect quenching was eventually larger than the size of the nonmetallic inclusions. Therefore, the fracture origins were mostly at the bainitic structure which is much softer than the martensite matrix. In this case, hydrogen is not concentrated around the bainitic structure.

Very recently (in the beginning of 2000) Murakami, Konishi and Takai [20] detected by SIMS the direct evidence of more hydrogen present at the nonmetallic inclusion of the fatigue fracture origin in the Specimens QT of SCM435 but less hydrogen at the inclusion in the Specimen VQ (see Fig. 12).

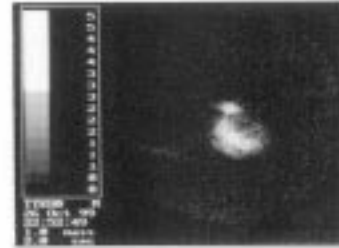


- : Specimen QT : Quenched and tempered
- ◆ : Specimen VA1 : Annealed in a vacuum at 300C for 1h after QT
- ▲ : Specimen VA2 : Annealed in a vacuum at 300C for 2h after QT
- △ : Specimen VQ : Quenched in a vacuum and tempered
- : Specimen QT : Tested under mean stress +300 MPa

Figure 11: A type 2 modified $S-N$ curve.
 σ = Stress amplitude.
 σ_w' = Fatigue limit calculated by the \sqrt{area} parameter model taking ODA into consideration.
The value of \sqrt{area} is evaluated to be equivalent to (ODA+inclusion size).
It is noted that ODA has a crucial role for eliminating the fatigue limit.



(a) Nonmetallic inclusion at fatigue fracture origin



(b) Hydrogen detected by SIMS at fracture origin

Figure 12: Evidence of hydrogen trapped by nonmetallic inclusion at fracture origin of Specimen QT [20].
 $\sigma = 561$ MPa, $N_f = 5.17 \times 10^7$, $\sqrt{area} = 31.0 \mu\text{m}$, $R = -1$

If we look at again Fig. 9 and compare the size of ODAs for Specimens QT and VQ, we can understand that the longer life for Specimen VQ than Specimen QT for the same value of ODA is due to the smaller hydrogen content in Specimen VQ which delays the fatigue crack growth up to the critical size for the mechanical fatigue threshold. The critical size of ODA for the crack growth without the assistance of hydrogen can be evaluated by using Eqn. (4) as

$$\sqrt{area}_c = [1.56(HV+120)/\sigma]^6 \quad (7)$$

where \sqrt{area}_c is the critical size of (ODA+inclusion) for the applied stress amplitude σ .

CONCLUSIONS

(1) Experimental evidences were shown that the hydrogen trapped by inclusions crucially influences both the threshold condition for fatigue failure in the superlong life regime of $N_f > 10^7$ cycles and the elimination of the conventional fatigue limit.

(2) Heat treated steels tend to have a high hydrogen content around inclusions. We need to consider this particular but important practical problem of fatigue failure in the regime of $N > 10^7$ cycles in structural design of high strength steels. Revising the existing design codes in terms of this problem is also necessary as suggested by Miller and O'Donnell [3].

REFERENCES

1. Naito, T., Ueda, H. and Kikuchi, M. (1984) *Met Trans.* **15A**, pp. 1431-1436.
2. Asami, K. and Sugiyama, Y. (1985) *J. Heat Treatment Technol. Assoc.* **25(3)**, pp. 147-150.
3. Miller, K. J. and O'Donnell, W. J. (1999) *Fatigue & Frac. Engng. Mat. Struc.* **22(7)**, pp. 545-557.
4. Murakami, Y., Nomoto, T. and Ueda, T. (1999) *Fatigue & Frac. Engng. Mat. Struc.* **22(7)**, pp. 581-590.
5. Kitagawa, H. and Takahashi, S. (1976) *Proc. 2nd Int. Conf. Mech. Behav. Mater.*, Boston pp. 627-631.

6. Murakami, Y. and Endo, T. (1980) *Int. J. Fatigue* **2(1)**, pp. 23-30.
7. Murakami, Y. (1993) *Metal Fatigue: Effects of Small Defects and Nonmetallic Inclusions*, Yokendo Ltd., Tokyo.
8. Murakami, Y., Nomoto, T., Ueda, T. and Murakami, Y. (1999) *submitted to Fatigue & Frac. Engng. Mat. Struc.*
9. Takai, K., Honma, Y., Izutsu, K. and Nagumo, M. (1996) *J. Japan Inst. Metals* **60-12**, pp. 1155-1162.
10. Takai, K., Seki, J., Yamauchi, G. and Honma, Y. (1994) *J. Japan. Inst. Metals*, **58-12**, pp. 1380-1385.
11. Heller, W. R. (1961), *Acta Metal.* **9**, pp. 600-613.
12. Au, J. J. and Birnbaum, H. K. (1973) *Scripta Metall.* **7**, pp. 595-604.
13. Clum, J. A. (1975) *Scripta Metall.* **9**, pp. 51-58.
14. Dufrense, J. F., Seeger, A., Groh, P. and Moser, M. (1976) *Phys. Status Solidi.* **36-a**, pp. 579-589.
15. Hagi, H., Hayashi, Y. and Ohtani, N. (1978) *J. Japan. Inst. Metals*, **42-2**, pp. 124-130.
16. Matsui, H. and Kimura, H. (1979) *Mater. Sci. Eng.* **40**, pp. 207-216.
17. Hirth, J. P. (1980) *Met. Trans. A.* **11A**, pp. 861-890.
18. Tabata, T. and Birnbaum, H. K. (1983) *Scripta Metall.* **17**, pp. 974-950.
19. Murakami, Y., Toriyama, T., Tsubota, K. and Furumura, K. (1998) *Bearing Steels: Into the 21st Century*, ASTM STP 1327, Hoo, J.J.C. and Green, W.B. (Eds). ASTM, pp. 87-105.
20. Murakami, Y., Konishi, H. and Takai, K., to be submitted somewhere.